Effect of sintering temperature on the microstructure and electrical properties of $(Na_{0.5}Bi_{0.5})TiO_3$ processed by the sol-gel method

M. Mesrar [1] · T. Lamcharfi[1] · N-S. Echatoui[1] · F. Abdi[1]

Abstract

$(Na_{0.5}Bi_{0.5})TiO_3$ lead free ceramics have been synthesised by conventional sol-gel reaction method. The crystalline phase of calcined ceramics was studied at room temperature using X-ray diffraction. Rietveld refinement of the XRD measurements by FullProf showed that the samples have a rhombohedral structure with a space group R3c. In this study, NBT ceramics were sintered at different temperatures of 1000 °C, 1050 °C and 1100 °C for a period of 4 h. The sintering temperature was determined to be 1100 C, and the effect of sintering temperature on grain size was interpreted using dynamic crystal growth theory and, consequently, the electrical behaviour was also examined. The dielectric properties of these ceramic products were examined at different temperatures over a wide frequency range using an impedance analyser. It was found that the dielectric constant and dielectric loss decreased with increasing measurement frequency. The resulting ceramics have a large maximum dielectric permittivity at 320 °C and a dispersive permittivity at high temperatures. The exposant critique ɣ of the relationship between the dielectric constant and temperature $\left(\varepsilon_{rmax/\varepsilon_r}\right)$ vs $(T-Tm)^{\gamma}$) has been calculated with precision for NBT relaxor ferroelectrics at different frequencies. The $(Na_{0.5}Bi_{0.5})TiO_3$ sample exhibits a diffuse ferroelectric behaviour.

Graphical abstract
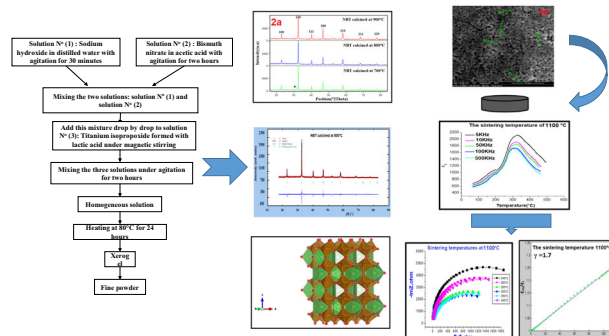
Highlights

- Lead-free piezoelectric ceramics $(Na_{0.5}Bi_{0.5})TiO_3$ are formed using the sol-gel method.
- The ceramics have a pure perovskite structure with the rhombohedral phase.
- Effects of sintering temperature on the electrical properties were investigated.
- The NBT exhibits ferroelectric relaxer behavior.

✉ M. Mesrar
mohammed.mesrar@usmba.ac.ma

1   Signals, Systems and Components Laboratory (LSSC), Faculty of Sciences and Technologies of Fez, Sidi Mohamed Ben Abdellah University, B.P. 2022 Fez, Morocco

1 Introduction

In today's electronic devices, perovskite materials occupy a large place, with wide applications. Their diversity in terms of structure and composition allows them to benefit from interesting properties such as piezoelectric, ferroelectric, electrostriction, pyroelectric, dielectric, etc [1–5]. The applications of ferroelectric materials are wide-ranging in piezoelectric, sensors, actuators and transducers. There are many applications for lead-based materials. An excellent example is PbTi1-xZrxO3 (PZT), which has outstanding ferroelectric properties [6–8]. PbO accounts for 60% of the weight of PZT. It is potentially toxic, highly volatile, and hazardous to human health and the environment [9, 10]. Global environmental concern resulted in a ban on lead-based electronic materials in 2008 [11]. As a result, stringent requirements for developing lead-free ferroelectric ceramic materials have been established [12–14]. In this regard, significant lead-free materials such as $(K_{0.5}Bi_{0.5})TiO_3$ (KBT) [15], $BaTiO_3$ (BT) [16, 17] and $(Na_{0.5}Bi_{0.5})TiO_3$ (NBT) [18–20] as well as their derived compositions have been developed for environmental reasons. Of the lead-free materials, NBT-based ceramics are particularly promising candidates. $(Na_{0.5}Bi_{0.5})TiO_3$ was first discovered by Smolenskii et al. in 1961 [21]. The material is of type ABO_3 with a disordered/mixed A-site. Pb^{2+}(6s2)-O2-(2p) hybridisation in $PbTiO_3$-based ferroelectric materials is analogous [9]. $(Na_{0.5}Bi_{0.5})TiO_3$ is characterised by Bi^{3+}(6s2)-O2-(2p) hybridisation. The Bi^{3+} ions are found in an isoelectronic configuration with Pb^{2+} [22]. Furthermore, Bi^{3+} ions have greater off-centreing capability than Pb^{2+} ions in a single unit cell. As a result, $(Na_{0.5}Bi_{0.5})TiO_3$ is a viable replacement for PZT compounds. With increasing temperature, it undergoes a structural phase transition from rhombohedral (Ferroelectric, Space group: R3c) to tetragonal (Antiferroelectric, Space group: P4bm) and tetragonal (Antiferroelectric) to cubic (Paraelectric, Space group: $Pm\overline{3}m$) [9, 23, 24]. $Na_{0.5}Bi_{0.5})TiO_3$ represents a ferroelectric material with a high remanent polarisation, Pr~38 C/cm², a correspondingly high depolarisation temperature, Td ~200 °C, and a high Curie temperature, Tc~320 °C. In the vicinity of the Curie temperature (Tc), the dielectric curves ε(T) broaden strongly with frequency, which explains their interest from a scientific and technical point of view. Furthermore, at Tc = Tm (the temperature at which the dielectric permittivity is maximum Ɛrmax), the NBT ceramic exhibits second order phase transitions, and these products are marked by the fact that the ε(T) curves are strongly deviated from the Curie–Weiss law [25]. The modified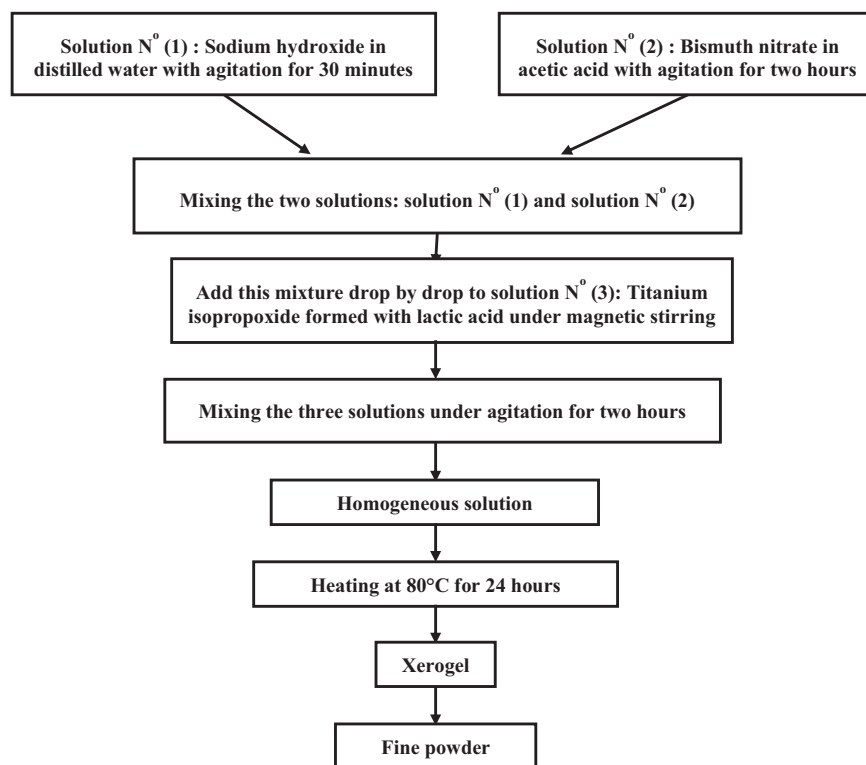 Curie–Weiss law can be used to define the diffusion of the ferroelectric phase transition. However, it has a high coercive field of 75 kV/cm a high leakage, which poses a problem during the polissing process [26, 27]. This limits the use of this material's piezoelectric properties in practical applications. In the recent years, extensive research has been carried out to develop NBT-based ceramics by various wet chemical methods, including the emulsion method [28], the citrate method [29], the solid state [19, 30], the hydrothermal process [31, 32] and sol-gel techniques [33, 34]. NBT-based ceramics made from powders synthesised by alternative methods were found to have better sintering ability, an improved process for polishing and better piezoelectric properties. In the present study, $(Na_{0.5}Bi_{0.5})TiO_3$ ceramics were produced by the sol-gel method [35–37], and their structural characteristics were determined using XRD and SEM measurements. Therefore, the aim of this paper is to investigate the effect of conventional sintering temperature (1000–1100 °C) on the phase composition, density, surface morphology and ferroelectric properties in order to obtain the best process parameters. The change in grain size with an increase of sintering temperature was explicated on the basis of dynamic growth theory of crystal [38]. In addition, the impact of the microstructure on the electrical properties of NBT ceramics was examined in detail. The remarkable electrical and optical properties of these materials make them ideal for use in ferroelectric and optical components.

2 Experiment

We, therefore, chose to use a hybrid alkoxide synthesis. It consists of a titanium alkoxide (titanium isopropoxide-Ti) associated with sodium hydroxide (NaOH) and bismuth salts (bismuth nitrate pentahydrate-$Bi(NO_3)_3.5H_2O$). The different synthesis steps are given in the flowchart in Fig. 1. Three solutions are prepared: Solution N° (1) is obtained by dissolving sodium hydroxide in distilled water. Solution N° (2) is obtained by dissolving bismuth nitrate in acetic acid.

Each of the above solutions is agitated until the salts are completely dissolved using a magnetic agitator. Titanium isopropoxide is formed with lactic acid under magnetic agitation and the result is solution N° (3). The two previous solutions (solution N° (1) and solution N° (2)) are mixed, and then this mixture is added to solution N° (3) drop by drop, while still maintaining magnetic agitation. The resulting mixture is then agitated for 2 h. Finally, a whitish, homogeneous viscous solution (gel) was obtained. The entire experiment was carried out at near room temperature. The resulting solution is dried at 80 °C for 24 h and then ground to powder using an agate

Fig. 1 Flow chart for the preparation of $(Na_{0.5}Bi_{0.5})TiO_3$ powder by the sol-gel process

```
┌─────────────────────────────────┐         ┌─────────────────────────────────┐
│ Solution Nᵒ (1) : Sodium hydroxide │         │ Solution Nᵒ (2) : Bismuth nitrate in │
│ in distilled water with agitation  │         │ acetic acid with agitation for two   │
│ for 30 minutes                     │         │ hours                                │
└─────────────────────────────────┘         └─────────────────────────────────┘
                      ↓                                ↓
        ┌───────────────────────────────────────────────────────┐
        │ Mixing the two solutions: solution Nᵒ (1) and solution Nᵒ (2) │
        └───────────────────────────────────────────────────────┘
                                    ↓
        ┌───────────────────────────────────────────────────────┐
        │ Add this mixture drop by drop to solution Nᵒ (3): Titanium │
        │ isopropoxide formed with lactic acid under magnetic stirring │
        └───────────────────────────────────────────────────────┘
                                    ↓
        ┌───────────────────────────────────────────────────────┐
        │ Mixing the three solutions under agitation for two hours │
        └───────────────────────────────────────────────────────┘
                                    ↓
                  ┌───────────────────────────┐
                  │   Homogeneous solution     │
                  └───────────────────────────┘
                                    ↓
                  ┌───────────────────────────┐
                  │ Heating at 80°C for 24 hours │
                  └───────────────────────────┘
                                    ↓
                        ┌───────────────┐
                        │    Xerogel     │
                        └───────────────┘
                                    ↓
                        ┌───────────────┐
                        │  Fine powder   │
                        └───────────────┘
```

mortar. Then, the powders were calcined at different temperatures (700 °C, 800 °C and 900 °C) during 4 h, in a high-purity alumina crucible using high temperature heat furnace. The product formed was deagglomerated by means of an agate mortar in the presence of a few drops of polyvinyl alcohol (PVA 3%) (binder and plasticizer). The products were compressed under uniaxial pressure to obtain pellets with a diameter of 12 mm and a thickness of about 1 mm, and under a pressure of 8 tons for 5 min, after which these pellets were sintered for 4 h at various temperatures ranging from 1000 °C to 1100 °C. The phase of the materials was analysed by X-ray diffraction on an X-ray diffractometer (XPERT-PRO with CuKα1 radiation $\lambda = 1.5406$) at a low scan speed of 2° min^{-1} throughout the extended Bragg angle range of $10° < 2\Theta < 80°$. Using the Rietveld method, crystallite sizes, weight fractions, lattice constants and crystalline fractions could be determined. The morphology and microstructure of the materials were studied using a scanning electron microscope (quanta 200, CURI laboratory in Fez). Dielectric measurements were carried out in the temperature (ambient −500 °C) and frequency (1 kHz-2 MHz) ranges by means of an impedance analyser (Agilent 4284 A). The measurements obtained in this way led us to determine the values of the capacitance parameters and to calculate the permittivity ($\varepsilon_r = C\, d/A\, \varepsilon_0$ where A the area of the cross-section of the pellet, C is the capacitance of the wafer, d is the thickness of the

wafer and $\varepsilon_0 = 8.85 \times 10^{12}$ F/m is the permittivity of the vacuum) as well as the dielectric loss of our as-treated materials. The piezoelectric determination was carried out using a theoretical calculation of the quasi-static piezoelectric constant.

3 Results and discussions

3.1 Structural analysis

Figure 2a presents the different X-ray diffractograms of our $(Na_{0.5}Bi_{0.5})TiO_3$ compounds prepared by the sol-gel route. All the diffractograms relating to this system were registered under the same operating conditions. The $(Na_{0.5}Bi_{0.5})TiO_3$ crystallises from 700 °C during 4 h, at which temperature all its characteristic peaks appear, while a low intensity peak at about 31.5° (marked by an asterisk) of secondary phase is present in the diffractogram which is difficult to identify. The diffractogram analysis of $(Na_{0.5}Bi_{0.5})TiO_3$ powder calcined at 800 and 900 °C for 4 h shows the formation of a pure perovskite phase, with no secondary phases present.

In addition, at 800 °C, the intensity and width at the half maximum of the most intense peak (110) appear to be narrower compared to the calcination temperature at 900 °C, hence at this temperature some changes (appearance of a shoulder) in the profile of the (111) peak can be

Fig. 2 a X-ray diffraction diagram of the sample $(Na_{0.5}Bi_{0.5})TiO_3$ calcined at different temperatures (700–800–900 °C). **b** Zoom of the (110) and (111) peak of the $(Na_{0.5}Bi_{0.5})TiO_3$ sample calcined at different temperatures (700, 800 and 900 °C)
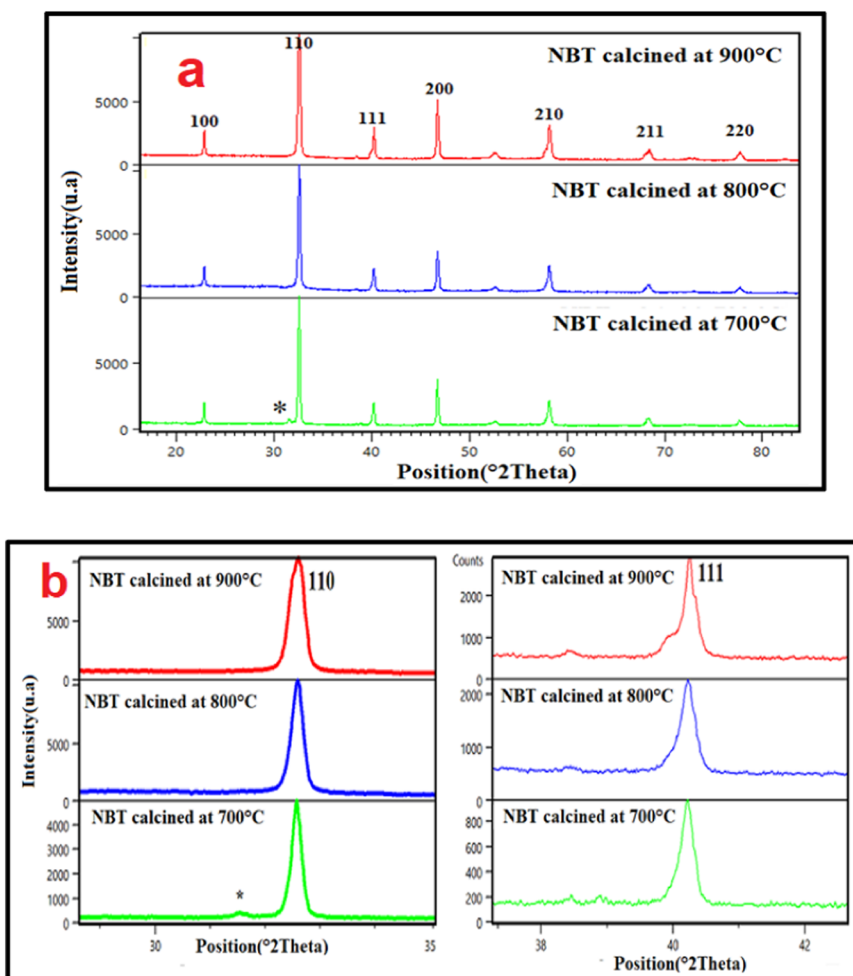
**Table 1** Lattice parameters of $(Na_{0.5}Bi_{0.5})TiO_3$

Lattice parameters	a (Å)	c (Å)	(c/a)	V (Å³)	Position (2θ) of the peak (110)	Average crystallite size (nm)	Space group
700 °C	5.5270	13.5341	2.4487	356.82	32.51	169.45	R3c
800 °C	5.5180	13.5292	2.4576	355.47	32.52	169.21	R3c
900 °C	5.5015	13.5206	2.4518	354.41	32.57	165.23	R3c

observed (Fig. 2b). Therefore, better crystallinity results are obtained for the sample calcined at 800 °C. For this purpose we studied the influence of the calcination temperature on the lattice parameters. Table 1 shows the influence of the calcination temperature on the crystalline parameters of the $(Na_{0.5}Bi_{0.5})TiO_3$ sample after calcination at different temperatures: 800 °C and 900 °C for 4 h, as well as the evolution of the position of the strongest line, the width at half-maximum (FWHM) and the average size of the crystallites calculated from the Debye-Scherrer formula by X'pertHighscore software [39]. The calculated crystal sizes for NBT calcined at (700, 800 and 900 °C) are 169.45, 169.21 and 165.23 nm, respectively, and

decrease with increasing temperature, while there is a slight increase in the lattice parameters. This can be attributed to the fact that the increase in calcination temperature broke down large crystallites with a single orientation into smaller crystallites with different orientations. There is also a slight difference in the position of the peaks, indicating the effect of the calcination temperature. We can therefore conclude that the calcination temperature of 800 °C for 4 h is sufficient for the complete crystallisation of our material.

In order to calculate the distances and the bond angles, we are using the Rietveld refinement to obtain the Cif* file used in the vesta software [40]. The refined XRD diagram

Fig. 3 Rietveld refinement patterns of ceramic samples calcined at 800 °C and 900 °C
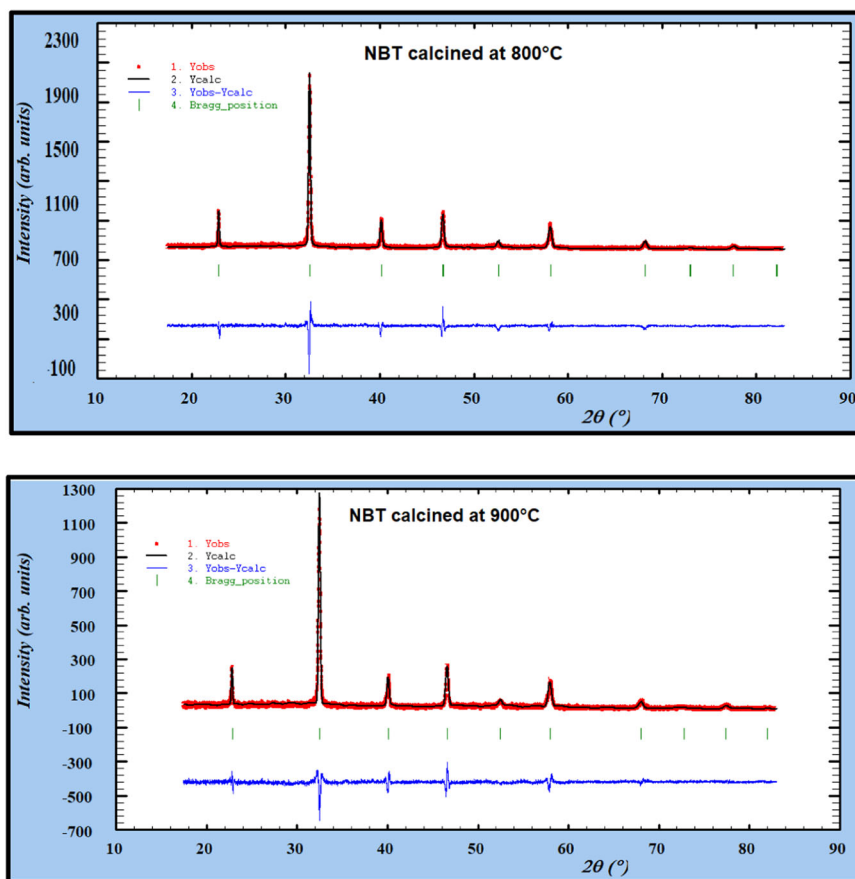
Table 2 Refined structural parameters along with profile R-factors for prepared samples

Atom	Site	x	y	z	B (Å)	Occupancy	Rietveld Parameters	χ^2	R_{EXP} (%)	R_{WP} (%)	R_P (%)
Na/Bi	6a	0	0	0.248	0.69	0.5/0.5	800 °C	1.20	1.43	1.72	1.11
Ti	6a	0	0	0.006	0.38	1	900 °C	1.97	1.21	2.39	1.14
O	18b	0.125	0.244	0.069	1.91	1	–		–	–	–	–

for all samples is presented in Fig. 3. This figure presents different types of lines for each graph.

The observed data is represented by the black line and the calculated data by the solid red line. The blue line shows the differences between the two types of data. The refined parameters of the lattice, R expected (R_{Exp}), weighted residual factor (R_{wp}), the profile factor (Rp) and the goodness of fit χ^2 are shown in Table 2. The refined values of these parameters are less than 2%, which lies between 1.20 and 1.97 and therefore it can be concluded that the data provided have an excellent fit. The final atomic parameters of the lattice sites (x, y, z), B(Å) and occupancy rate of atom were also calculated through the simulation for the NBT phase formed at the temperature of 800 °C. In this particular model, Na^+, Bi^{3+} and Ti^{4+} are situated at sites 6a (0, 0, z), Ti^{4+} cations also occur at positions 6a (0, 0, z), and oxygen atoms exist at general positions 18b (x, y, z).

Table 3 Bond angles and bond distance for all the synthesised products determined from Rietveld refinement

Samples	Bond distances (Å)	Bond angles (degree)
800 °C	Na/Bi–O = 2.7421, 2.6870, 2.6724 Ti–O = 2.3254, 1.8521	Ti–O–Ti = 169.2
900 °C	Na/Bi–O = 2.6025, 2.6234, 2.61514 Ti–O = 2.24325, 1.78532	Ti–O–Ti = 156.1

Table 3 presents the bond distances and angles calculated using Rietveld refinement, where Na/Bi-O and Ti-O represent the bond distances of $(Na_{0.5}Bi_{0.5})TiO_3$ site A and B ions for both samples. Thus, bond lengths average value is calculated to be around 2.70 Å for NBT formed at 800 °C. In addition, a slight decrease in the distance and bond angles is observed by increasing the calcination temperature. Hence,

Fig. 4 **a**, **c** and **e** SEM picture of specimen sintered at 1000 °C for 4 h; **b**, **d** and **f**) presents its grain size
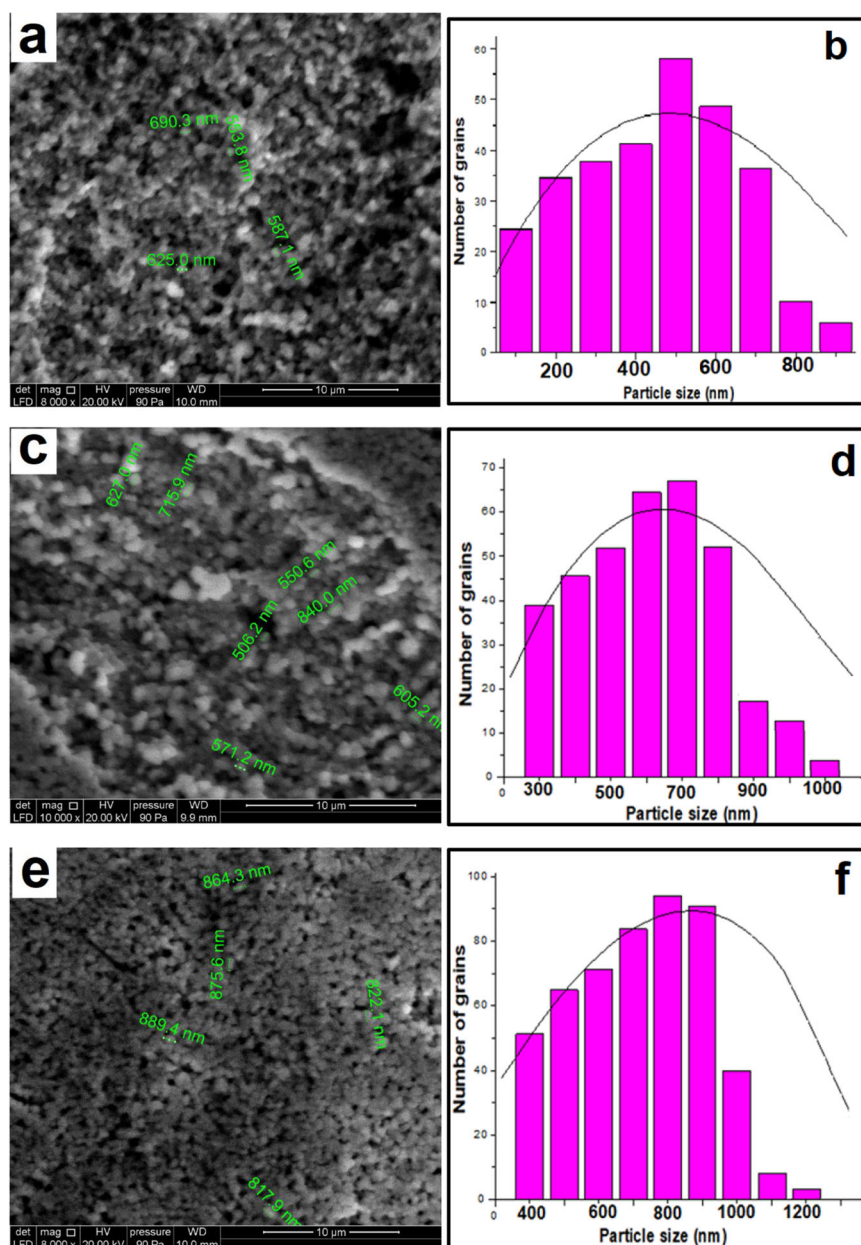
the unit cell of the rhombohedral phase decreases and the crystallite size decreases from 169.21 nm to 165.23 nm for a temperature of 900 °C, as mentioned in Table 2 Therefore, increasing the calcination temperature leads to lattice strain, which may lead to to deficiencies in the sub-lattice that will affect the stability of the overall system. These results permit to obtain the confirmation of the internal stresses present in the structure.

3.2 Scanning electron microscopy study (SEM)

The microstructure of $(Na_{0.5}Bi_{0.5})TiO_3$ ceramics prepared by the sol-gel process was examined using a scanning electron microscope (SEM). Figure 4a, c, e shows the SEM images of the sintered NBT samples at different temperatures 1000 °C, 1050 °C and 1100 °C. These samples display clearly visible grains and grain boundaries, suggesting the polycrystalline nature of the specimens. The microstructure is relatively dense and one can observe spherical grains and partial intergranular pores. To calculate the average diameter of the NBT grains, the free image treatment software ImageJ [41, 42] has been used, through which the perimeter of each of the NBT grains that can be visualised in the images was plotted (Fig. 4b, d, f), and with this computation, the software finds the area of each grain. Then, the grain diameter is determined. This counts and draws the histogram of the diameter of the grains that make up the NBT image, as illustrated in Fig. 4a, c, e. For each

Table 4 Grain size and apparent activation energy of materials sintered at 1000–1100 °C

T (°C)	1000	1050	1100
G (nm)	540.61	732.67	835.52
Q (Kj/mol)	−114	137	182
Experimental Density (g/cm³)	5.14	5.29	5.98

histogram (the percentage of the number of gains according to their diameter) presented in figure Fig. 4b, d, f, a Gaussian distribution has been adjusted, which is displayed by the black solid line whose maximum position corresponds to the average grain size for every perovskite picture. The average grain size of the NBT image for all sintering temperatures are grouped in Table 4. Figure 4a shows a less compact microstructure with the presence of a few porosity and Fig. 4b presents the characteristics of the sample and indicates the grain size distribution in the sample sintered at 1000 °C for 4 h in the usual way with an average grain size of about ~ (540.61 nm). The picture 4(c) illustrates a compact microstructure with a low amount of porosity and the corresponding size distribution of the granules is illustrated in Fig. 4d for the sample sintered at 1050 °C for 4 h, which is more uniform than the other sintered samples and the histogram shows that the average granule size increases ~ (732.67 nm) as against the conventional sample sintered at 1000 °C. Figure 4e exhibits a microstructure with very low porosity and the grain distribution reveals a further increase in the average grain size ~ (835.52 nm) as illustrated in Fig. 4f for the sample sintered at 1100 °C for 4 h. It can be seen that the average grain size has significantly increased and that sintering at temperatures of about 1100 °C for 4 h accelerates the growth of the grains in the considered system. The histograms of the grains revealed that the specimen treated with sintering at 1100 °C for 4 h had the most uniform distribution of grains in the 700 nm to 900 nm range, compared to the specimen sintered at lower temperatures, as reported in Table 4.

distribution. (c) SEM picture of a specimen sintered at 1050 °C for 4 h;(d) represents the distribution of grains in relation to their size. (d) shows the grain size distribution. (e) SEM picture of a sample sintered at 1100 °C for 4 h; (f) presents its grain size distribution. The grain size becomes larger as the sintering temperature rises, which makes it possible to correlate the coarsening behaviour of the grains. Similarly, some anomalous grains were observed in the samples sintered at 1000 °C, 1050 °C and 1100 °C. The overall changes in shape, size and surface of the grain boundaries are expected to influence the transport properties which will be examined in the next section. The theory of dynamic crystal growth (formula (1)) also provides an explanation for the variation in particle size [38, 43]. Appearant activation energy (Q) is the motive

force for grain growth, so the higher its value, the more rapid the grain growth. The Qs of the materials (1000–1100 °C) were determined and reported in Table 4. The positive Q (1000–1100 °C) allowed us to follow grain size growth. The compound sintered at (1100 °C) with Q_{max} has the maximum energy at the grain boundaries, whereby the grain size of compound (1100 °C) becomes maximum. The reduction in grain size of the material (1000 °C) is explained by the negative Q. Consequently, it is very important to select an adequate sintering process to yield an excellent NBT compound.

$$G^n - G_0^n = K_0 - t. \exp\left(-\frac{Q}{RT}\right) \tag{1}$$

in which G_0^n is the original grain size, G^n is the grain size, T represents the temperature of the reaction, t is reaction time, R nd K_0 are considered constant, and n represents the dynamic grain growth index.

3.3 Dielectric measurements

Dielectric measurements were carried out on sintered ceramics at different temperatures (1000 °C, 1050 °C and 1100 °C) for 4 h. Figure 5 displays the curve of the relative permittivity (εr) as a function of temperature at various measured frequencies (5kHz–500kHz). The dielectric constant ($\varepsilon_{rmax} = 2100$; 5 kHz) reaches the maximum value at low frequencies, then decreases along with the frequency and attains constant values with the highest frequencies. At low frequencies, however, the higher dielectric constant is mainly due to the existence of all types of polarisation [44]. The transition from the ferroelectric to the paraelectric phase appears for all NBT sample.

According to Fig. 5, the permittivity increases with the increase of the temperature; it passes through a maximum value (ε_{rmax}) for $T = T_m$ and then decreases. The curves obtained reveal two dielectric anomalies. These are attributed to phase transitions:

- An anomaly translated by a shoulder, observed around 200 °C, which corresponds to the intermediate transition (ferroelectric-antiferroelectric) [45]. The temperature corresponding to this transition is called the depolarisation temperature (Td), because at this temperature the sample is essentially depolarised and loses its piezoelectric activity. These temperatures were taken as an indication of the temperature stability of the ferroelectric domains [46].
- The second anomaly observed near 340 °C; is a broad peak that corresponds to a maximum of the dielectric constant. This anomaly corresponds to the antiferroelectric to paraelectric transition. The temperature that corresponds to the maximum value of the dielectric

Fig. 5 Dielectric constant values of $(Na_{0.5}Bi_{0.5})TiO_3$ compounds prepared sol-gel and sintered at 1000 °C, 1050 °C and 1100 °C for 4 h as a function of temperature at different frequencies
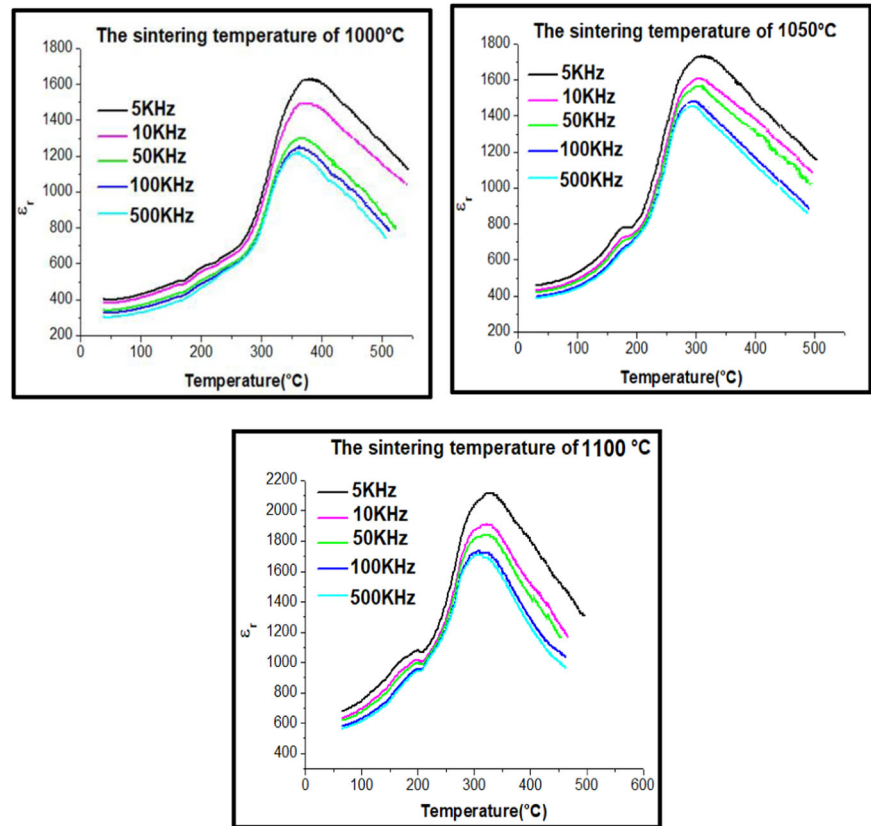
constant is called the maximum temperature (T_m) [47]. The maximum of the permittivity around 340 °C is large; it covers a large temperature range. This anomaly is normally associated with the transition to the paraelectric state. The diffusive character of the material is thus confirmed.

Increasing the sintering temperature leads to an increase in the dielectric constant of NBT. Dielectric constant values of NBT, which are measured at a frequency of 5 kHz for samples at a sintering temperature of 1000 °C, 1050 °C, and 1100 °C were found to be 1605, 1725, and 2100, respectively. In ferroelectric product polycrystals, there exist domains. The domain is the area that has polarisation in the same direction. The domains get larger as the grains size increases, hence, the polarisation will become stronger. This suggests that the dielectric constant of NBT is increasing [48, 49].

3.4 Complex impedance study

The complex impedance modelling technique is a highly efficient technique that aims to distinguish between grain boundary and grain electrode effects, which are typically where defects and oxygen vacancies are captured. In addition, it is interesting to establish a real picture of the polarisation and relaxation process of space charges by assigning different measures of capacitance and resistance to boundary and grain effects to the material concerned. This technique is also used to reveal the influences of grains (intrinsic), grain boundaries (extrinsic) and the interface between the electrode and the sample on the electrical properties (i.e., transport properties) and to correlate them with the morphology of the samples examined. The principle of this method is based on the calculation of the AC response of a device to a sinusoidal disturbance. Then the impedance is determined with respect to the frequency of the perturbation. To distinguish grain effects from grain boundary effects, the complex impedance curves made at several temperatures for all compounds. Depending on the electrical characteristics of the material under examination, it can be seen that the Nyquist curves are usually marked with three semicircles, which appeared when the grain boundary resistance was dominant compared to the overall resistance. This situation most often occurs because grain boundaries contain high densities of structural and chemical defects, for which the charge carriers have difficulty moving as a function of the external field exerted. It thus reveals the setting up of a potential barrier preventing the formation of precipitates or favouring the accumulation of defects on the surface of the grains.

Therefore, compared to the carriers inside the grains, the latter have a strong possibility to relax at lower frequencies (i.e., for a longer time). As a result, the rather large

Fig. 6 Im Z vs Real Z curve of specimens sintered at 1000 °C, 1050 °C and 1100 °C for 4 h
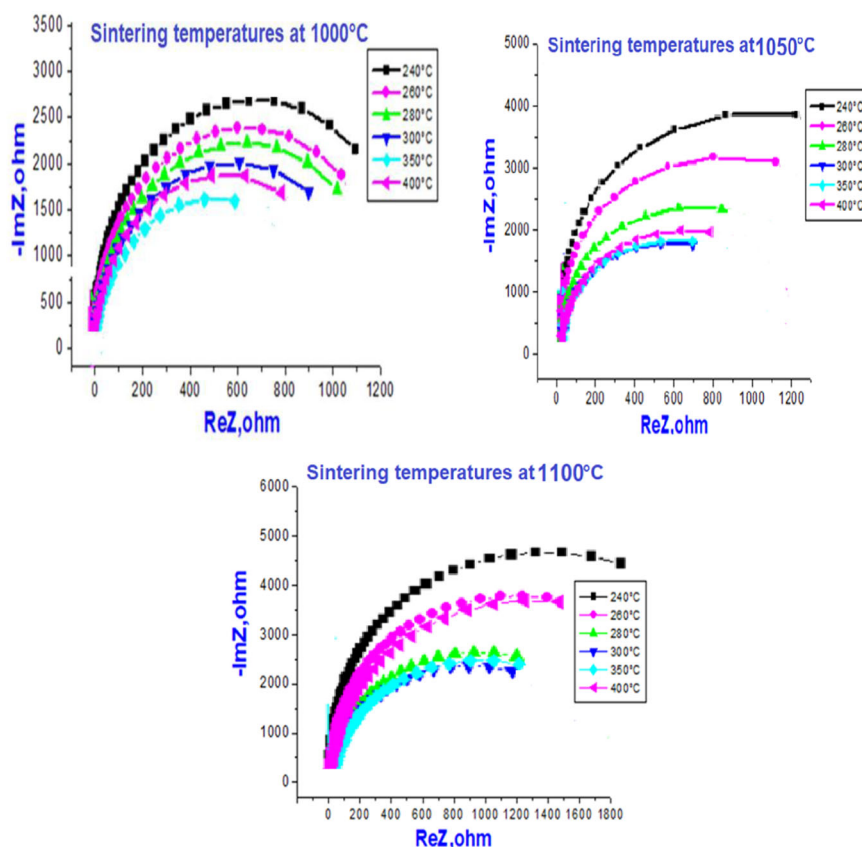
semicircle that appears at lower frequencies with higher resistance values is assigned to the boundaries of the grains that behave as insulators, while the semicircle on the side of higher frequencies is assigned to the grains with lower internal resistance that behave as semiconductors. The Cole-Cole spectra (-Im Z Vs. Real Z) of $(Na_{0.5}Bi_{0.5})TiO_3$ materials sintered during 4 h for different temperatures 1000 °C, 1050 °C and 1100 °C in the temperature range 240–400 °C have been presented in Fig. 6. The curves are in the form of a semicircle with the centres below the actual Z axis. The results show an assignment of the relaxation time (i.e., $\omega = 2\pi f_{max} = 1/\tau$) and highlight a clear deviation from the Debye type relaxation. The semi-circular arcs were identified in the temperature range of 240–400 °C, as illustrated in Fig. 5. For temperatures in the region of 240–400 °C, the involvement of the inside of the grain could be favoured. However, as the sintering temperature increases, the grain strength limits increase, which could be related to the decrease in defect compactness. This was also validated by SEM analysis. In the figure (Fig. 6), the Cole-Cole curve at 400 °C with different sintering temperatures has been plotted. In this curve, we observed that the radius of the semicircle increased with increasing sintering temperature, which corresponds to an increase in the impedance value. This phenomenon may be another reason for the decrease in the conductivity value. Singha et al. mentioned the same

type of behaviour in materials obtained after long-term sintering [45, 50]. This result could be attributed to the predominance of the grain interior resulting in a reduction in grain boundary participation, which allowed for significant grain growth, as demonstrated by SEM micrographs.

3.5 Transition diffuseness

The appearance of a ferroelectric phase is the consequence of structural phase transitions. These transitions take place within a temperature range, which can reach several tens of degrees, so both phases coexist in this region. These transitions are then best described using a critical temperature distribution. The presence of a diffuse transition is thought to be related to material defects such as stoichiometry fluctuations, granularity and structural disorder.

To define the behaviour of the material and to highlight the diffuse character of the transition, a modification of Uchino's law has been proposed by N.S. Echatoui et al. [51] to describe the diffuse transition by the following relation:

$$\frac{1}{\varepsilon_r} = \frac{1}{\varepsilon_{r\,max}} \left[1 + \frac{(T - T_m)^\gamma}{2\delta^\gamma} \right] \qquad (2)$$

With:

$\varepsilon_{r\,max}$: Dielectric constant at the maximum temperature T_m.
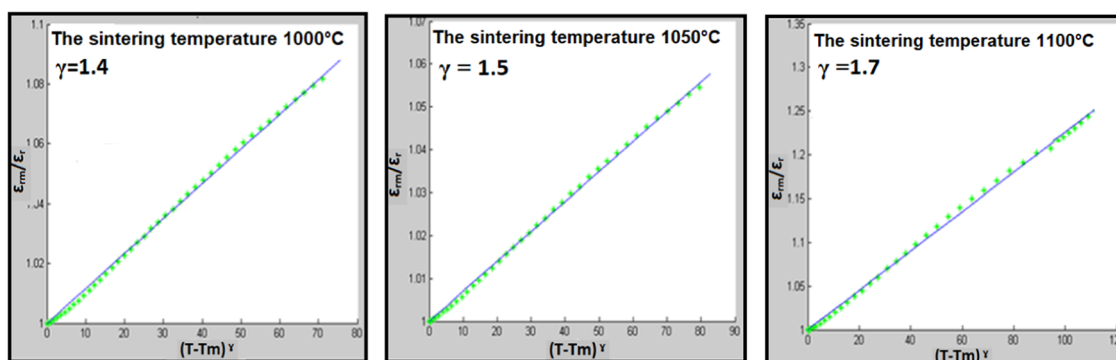
Fig. 7 Plot of $\left(\varepsilon_{\mathrm{rmax}/\varepsilon_r}\right)$ as a function of $(T-Tm)^{\gamma}$ at 10 kHz for $(Na_{0.5}Bi_{0.5})TiO_3$

Table 5 $(Na_{0.5}Bi_{0.5})TiO_3$ parameter values (γ and δ) at 10 kHz

Sintering temperature (°C)	γ	δ
1000	1.4	95
1050	1.5	107
1100	1.7	125

γ: Constant, between 1 (normal ferroelectric) and 2 (relaxor) whose value reflects the more or less diffuse character of the transition in the material.

The curve of $\left(\varepsilon_{\mathrm{rmax}/\varepsilon_r}\right)$ versus $(T-Tm)^{\gamma}$ of the $(Na_{0.5}Bi_{0.5})TiO_3$ sample at 10 kHz is shown in Fig. 7. A linear dependence between the two logarithmic quantities is evident regardless of the sintering temperature. The γ values are systematically calculated from the slope of each curve and are equal to 1.4, 1.5 and 1.7 for sintering temperatures of 1000 °C, 1050 °C and 1100 °C respectively. Therefore, the different compounds studied show a diffuse phase transition which approaches the relaxor behaviour in the case of $\gamma = 1.7$ for the sintering temperature of 1100 °C. The values of the diffusion factor δ are shown in Table 5. It can clearly be observed that as the sintering temperature increases, the δ factor also increases, which implies that the transition becomes more and more diffuse, so logically the variation of γ should evolve in the same direction as δ.

The diffuse behaviour is probably attributed to the random distribution of cations within the A-site, which induces a charge imbalance due to substitution by different charge at the A-site (Na^+/Bi^{3+}). These results support those of dielectric measurements already reported in the literature [46, 52–54].

4 Conclusion

$(Na_{0.5}Bi_{0.5})TiO_3$ ceramics were developed by the sol-gel method to study the influence of sintering temperature on the ferroelectric properties of $(Na_{0.5}Bi_{0.5})TiO_3$ samples. The

XRD plot of the obtained samples reveals a unique rhombohedral phase structure with a hexagonally symmetric R3C space group. The evolution of the position of the strongest line (110), the width at half maximum (FWHM) and the average crystallite size decreases with increasing calcination temperature (from 800 to 900 °C) while there is a slight increase in lattice parameters. The results of the microstructure analysis showed that the grain size and growth were enhanced with increasing sintering temperature. The results of the grain histogram analysis reveal that the maximum grain distribution in the range of 700 nm to 900 nm was found in the sample developed from a sintering temperature of 1100 C for 4 h. The reduced grain size of the sintered samples at 1000 °C is explained by the diffusion and fusion of small holes at the grain boundaries. The increase in the dielectric constant at the highest sintering temperature (1100 °C) indicates an improvement in the relaxation property of the ceramics concerned. The Cole-Cole diagrams obtained are all arcs or semicircles for all samples. Thus, the centre of the semicircles is below the real axis, which shows that the relaxation of the materials is not Debye. A diffusive character study was carried out to understand the variation of the dielectric behaviour and its relation to the sintering temperature. The calculated γ coefficient is 1.7, which means that the material has relatively moderate relaxation characteristics.

Compliance with ethical standards

References

1. Zhang S, Alberta EF, Eitel RE, Randall CA, Shrout TR (2005) "Elastic, piezoelectric, and dielectric characterization of modified BiScO$_3$-PbTiO$_3$ ceramics,". IEEE Trans Ultrason Ferroelectr Freq

Control 52(11):2131–2139. https://doi.org/10.1109/TUFFC.2005.1561684

2. Cross LEric (1987) "Relaxor ferroelecirics,". Ferroelectrics 76(1):241–267. https://doi.org/10.1080/00150198708016945

3. Mesrar M, Lamcharfi T, Echatoui N-S, and Abdi F (2022) "(1-x)(Na$_{0.5}$Bi$_{0.5}$)TiO$_{3-x}$(K$_{0.5}$Bi$_{0.5}$)TiO$_3$ ceramics near morphotropic phase boundary: a structural and electrical study," Materialia 101404.https://doi.org/10.1016/J.MTLA.2022.101404

4. Chanda S, Maity R, Saha S, Dutta A, Sinha TP (2021) "Double perovskite nanostructured Dy$_2$CoMnO$_6$ an efficient visible-light photocatalysts: synthesis and characterization,". J Sol-Gel Sci Technol 99(3):600–613. https://doi.org/10.1007/S10971-021-05605-Y/TABLES/3

5. Madhan K, Murugaraj R (2020) "Structural, electrical, and weak ferromagnetic-to-antiferromagnetic nature of Ni and La co-doped BaTiO$_3$ by sol–gel combustion route,". J Sol-Gel Sci Technol 95(1):11–21. https://doi.org/10.1007/S10971-020-05311-1

6. Ozer N, Sands T (2000) "Preparation and optical characterization of sol-gel deposited Pb(Zr$_{0.45}$Ti$_{0.55}$)O$_3$ films,". J Sol-Gel Sci Technol 19(1–3):157–162. https://doi.org/10.1023/A:1008711632646

7. Binkle O, Nass R (1998) Synthesis and Characterization of PZT Fibers via Sol-Gel J. Sol-Gel Sci.Technol 13(1):1023–1026. https://doi.org/10.1023/A:1008616516686

8. Zhang J, Zhang Y, Yan Z, Wang A, Jiang P, Zhong M (2020) "Fabrication and performance of PNN-PZT piezoelectric ceramics obtained by low-temperature sintering,". Sci Eng Compos Mater 27(1):359–365. https://doi.org/10.1515/SECM-2020-0039/MACHINEREADABLECITATION/RIS

9. Verma A et al. (2019) Enhanced energy storage properties in A-site substituted Na$_{0.5}$Bi$_{0.5}$TiO$_3$ ceramics. J Alloy Compd 792:95–107. https://doi.org/10.1016/j.jallcom.2019.03.304

10. Yang Y et al. (2021) "Enhancement of magnetoresistance and near room-temperature temperature coefficient of resistivity in polycrystalline La$_{0.7}$Ca$_{0.24}$Na$_{0.06}$MnO$_3$ by silver doping,". J Sol-Gel Sci Technol 99(3):627–635. https://doi.org/10.1007/S10971-021-05614-X/FIGURES/7

11. Shrout TR, Zhang SJ (2007) "Lead-free piezoelectric ceramics: Alternatives for PZT?,". J Electroceram 19(1):111–124. https://doi.org/10.1007/s10832-007-9047-0

12. Otoničar M, Škapin SD, Spreitzer M, Suvorov D (2010) "Compositional range and electrical properties of the morphotropic phase boundary in the Na$_{0.5}$Bi$_{0.5}$TiO$_3$-K$_{0.5}$Bi$_{0.5}$TiO$_3$ system,". J Eur Ceram Soc 30(4):971–979. https://doi.org/10.1016/j.jeurceramsoc.2009.10.006

13. Yang Z et al. (2019) Grain size engineered lead-free ceramics with both large energy storage density and ultrahigh mechanical properties. Nano Energy 58:768–777. https://doi.org/10.1016/j.nanoen.2019.02.003

14. Madhan K, Jagadeeshwaran C, Murugaraj R (2019) "Enhancement of electrical and magnetic properties in acceptor-doped BaTiO$_3$ ferroelectric ceramics,". J Mater Sci Mater Electron 30(3):2953–2965. https://doi.org/10.1007/S10854-018-00573-6

15. Liu G, Jiang W, Zhang L, Cai J, Wang Z, Liu K, ... Yan Y (2018) Effects of sintering temperature and KBT content on microstructure and electrical properties of (Bi$_{.5}$Na$_{.5}$)TiO$_3$-BaTiO$_3$-(Bi$_{.5}$K$_{.5}$)TiO$_3$ Pb-free ceramics. Ceramics International, 44(8):9303–9311

16. Madhan K, Murugaraj R (2020) "Enrichment of optical, electrical, and magnetic properties of Li+, La3+ doped BaTiO$_3$ perovskite multifunctional ceramics," Appl Phys A Mater Sci Process, 126(2) https://doi.org/10.1007/S00339-020-3285-2

17. Madhan K, Selvadurai APB, Murugaraj R (2019) Conjuring of defect-induced short and long-range ferromagnetism ordering in Ba$_{(1-x)}$Nd$_x$Ti$_{0.99}$Co$_{0.01}$O$_3$. Materials Letters 243:100–103

18. Elkechai O, Manier M, Mercurio JP (1996) "Na$_{0.5}$Bi$_{0.5}$TiO$_3$-K$_{0.5}$Bi$_{0.5}$TiO$_3$ (NBT-KBT) system: A structural and electrical study,". Phys Status Solidi Appl Res 157(2):499–506. https://doi.org/10.1002/pssa.2211570234

19. Sidi MM, Ben M, and Sidi FA (2018) "Investigation of Morphotropic Phase Boundary by Rietveld Refinement and Raman Spectroscopy for (1-x)(Na$_{0.5}$Bi$_{0.5}$)TiO$_{3-x}$BaTiO$_3$ Ceramics ASIAN JOURNAL OF CHEMISTRY ASIAN JOURNAL OF CHEMISTRY,". https://doi.org/10.14233/ajchem.2018.21116

20. Fang X, Shen B, Zhai J, Yao X (2011) "Preparation, dielectric and ferroelectric properties of (Na$_{0.5}$Bi$_{0.5}$)$_{0.94}$Ba$_{0.06}$TiO$_3$ thin films by a sol-gel process,". J Sol-Gel Sci Technol 58(1):1–5. https://doi.org/10.1007/S10971-010-2346-Y/FIGURES/7

21. Smolenskii GA, Chupis IE (1982) "Ferroelectromagnets,". Sov Phys - Uspekhi 25(7):415–448. https://doi.org/10.1070/PU1982v025n07ABEH004570

22. Yadav AK et al. (2017) "Structural and dielectric properties of Pb$_{(1-x)}$(Na$_{0.5}$Sm$_{0.5}$)$_x$TiO$_3$ ceramics,". J Mater Sci Mater Electron 28(14):10730–10738. https://doi.org/10.1007/s10854-017-6849-y

23. Jones GO, Thomas PA (2002) "Investigation of the structure and phase transitions in the novel A-site substituted distorted perovskite compound Na$_{0.5}$Bi$_{0.5}$TiO$_3$,". Acta Crystallogr Sect B Struct Sci 58(2):168–178. https://doi.org/10.1107/S0108768101020845

24. Li LQ, Xiong Y, Tang MH, Cheng CP, Ouyang J (2014) "Effect of BiFeO$_3$ doping on ferroelectric properties of Na$_{0.5}$Bi$_{0.5}$TiO$_3$–BaTiO$_3$ based thin film derived by sol–gel method,". J Sol-Gel Sci Technol 72(2):394–397. https://doi.org/10.1007/S10971-014-3448-8/FIGURES/3

25. Puli VS, Martínez RV, Kumar A, Scott JF, Katiyar RS (2011) "A quaternary lead based perovskite structured materials with diffuse phase transition behavior,". Mater Res Bull 46(12):2527–2530. https://doi.org/10.1016/j.materresbull.2011.08.017

26. Raghavender M, Kumar GS, Prasad G (2009) "A-site substitution-controlled dielectric dispersion in lead-free sodium bismuth titanate,". Pramana - J Phys 72(6):999–1009. https://doi.org/10.1007/s12043-009-0092-x

27. Kreisel J, Glazer AM, Bouvier P, Lucazeau G (2001) "High-pressure Raman study of a relaxor ferroelectric: The Na$_{0.5}$Bi$_{0.5}$-TiO$_3$ perovskite,". Phys Rev B—Condens Matter Mater Phys 63(17):1741061–17410610. https://doi.org/10.1103/physrevb.63.174106

28. Bibi I et al. (2021) Effect of dopant on ferroelectric, dielectric and photocatalytic properties of chromium-doped cobalt perovskite prepared via micro-emulsion route. Results Phys 20:103726. https://doi.org/10.1016/J.RINP.2020.103726

29. Hanžić N, Jurkin T, Maksimović A, Gotić M (2015) "The synthesis of gold nanoparticles by a citrate-radiolytical method,". Radiat Phys Chem 106:77–82. https://doi.org/10.1016/J.RADPHYSCHEM.2014.07.006

30. Mielewczyk-Gryn A et al. (2013) Characterization of CaTi$_{0.9}$Fe$_{0.1}$O$_3$/La$_{0.98}$Mg$_{0.02}$NbO$_4$ composite. Cent Eur J Phys 11(2):213–218. https://doi.org/10.2478/s11534-012-0152-6

31. Mesrar M, Lamcharfi T, Echatoui N-S, Abdi F, and Harrach A (2019) "High dielectric constant of (1-x)(Na$_{0.5}$Bi$_{0.5}$)TiO$_{3-x}$BaTiO$_3$ prepared by the hydrothermal method," Mediterr J Chem. https://doi.org/10.13171/10.13171/mjc8319051210mm

32. Aman D, El-Hafiz DRA, Ebiad MA(2018) "Thermodynamic parameter for steam reforming reaction of biodiesel by-product using nano-sized perovskite catalysts," Moroccan J Chem 6(3):466–479. https://doi.org/10.48317/IMIST.PRSM/MORJCHEM-V6I3.6444

33. Madhan K, Murugaraj R (2020) "Investigation on microstructural, electrical and optical properties of Nd-Doped BaCo$_{0.01}$Ti$_{0.99}$O$_3$ perovskite,". J Electron Mater 49(1):377–384. https://doi.org/10.1007/s11664-019-07751-0

34. Cernea M, Vasile BS, Capiani C, Ioncea A, Galassi C (2012) "Dielectric and piezoelectric behaviors of NBT-BT$_{0.05}$ processed by sol-gel method,". J Eur Ceram Soc 32(1):133–139. https://doi.org/10.1016/j.jeurceramsoc.2011.07.038

35. Fu Z, Zhu R, Wu D, Li A (2008) "Preparation of $(1-x\%)$ $(Na_{0.5}Bi_{0.5})TiO_{3-x}\%SrTiO_3$ thin films by a sol–gel method for dielectric tunable applications," J Sol-Gel Sci Technol 49(1):29–34. https://doi.org/10.1007/S10971-008-1844-7

36. Li LQ, Xiong Y, Tang MH, Cheng CP, Ouyang J (2014) "Effect of $BiFeO_3$ doping on ferroelectric properties of $Na_{0.5}Bi_{0.5}TiO_3$–$BaTiO_3$ based thin film derived by sol–gel method," J Sol-Gel Sci Technol 72(2):394–397. https://doi.org/10.1007/S10971-014-3448-8

37. Fang X, Shen B, Zhai J, Yao X (2010) "Preparation, dielectric and ferroelectric properties of $(Na_{0.5}Bi_{0.5})_{0.94}Ba_{0.06}TiO_3$ thin films by a sol–gel process," J Sol-Gel Sci Technol 58(1):1–5. https://doi.org/10.1007/S10971-010-2346-Y

38. Wang Q, Lian G, Dickey EC (2004) "Grain boundary segregation in yttrium-doped polycrystalline TiO_2,". Acta Mater 52(4):809–820. https://doi.org/10.1016/j.actamat.2003.10.016

39. Philips Analytical (2001) "New analytical software for XRD simplifies identification of complex phase mixtures. J Appl Crystallogr 34(6):788–788. https://doi.org/10.1107/s0021889801019264

40. Rodríquez-Carvajal J, Roisnel T (2004) Line broadening analysis using FullProf*: determination of microstructural properties. In Materials Science Forum (Vol. 443, pp. 123–126). Trans Tech Publications Ltd

41. Schneider CA, Rasband WS, Eliceiri KW(2012) "NIH Image to ImageJ: 25 years of image analysis," Nat Methods 9(7):671–675. https://doi.org/10.1038/nmeth.2089

42. Igathinathane C, Pordesimo LO, Batchelor WD (2009) "Major orthogonal dimensions measurement of food grains by machine vision using ImageJ,". Food Res Int 42(1):76–84. https://doi.org/10.1016/J.FOODRES.2008.08.013

43. Taïbi-Benziada L, Simon A (2009) "Sintering, microstructures and dielectric properties of Ba_{1-x} $Pb_x(Ti_{1-x}Li_x)O_{3-3x}$ F_{3x} ferroelectric ceramics,". Cent Eur J Chem 7(2):159–163. https://doi.org/10.2478/s11532-008-0063-y

44. Dagar S, Hooda A, Khasa S, Malik M (2020) "Investigations of structural, enhanced dielectric and magnetic properties of NBT doped ferrite system,". Mater Chem Phys 249:123214. https://doi.org/10.1016/J.MATCHEMPHYS.2020.123214

45. Mesrar M, Lamcharfi T, Echatoui N-S et al. (2019) High dielectric constant of (1-x)(Na0. 5Bi0. 5) TiO3-xBaTiO3 prepared by the hydrothermal method. Mediterranean Journal of Chemistry 8(3):213–219

46. Mesrar M, Lamcharfi T, Echatoui N, Abdi F, Harrach A, Ahjyaje FZ (2019) "Hydrothermal synthesis, microstructure and electrical properties of $(1-x)(Na_{0.5}Bi_{0.5})TiO_{3-x}BaTiO_3$ ceramics,". Moroccan J Quant Qual Res 0(1):14–24

47. Roukos R, Dargham SA, Romanos J, Barakat F, Chaumont D (2019) "Complex structural contribution of the morphotropic phase boundary in $Na_{0.5}Bi_{0.5}TiO_3$—$CaTiO_3$ system,". Ceram Int 45(4):4467–4473. https://doi.org/10.1016/j.ceramint.2018.11.126

48. Dunce M et al. (2021) Influence of sintering temperature on microstructure of $Na_{0.5}Bi_{0.5}TiO_3$ ceramics. J Alloy Compd 884:160955. https://doi.org/10.1016/J.JALLCOM.2021.160955

49. Bhattacharyya R, Das S, Das A, Omar S (2021) "Effect of sintering temperature on the microstructure and conductivity of $Na_{0.54}Bi_{0.46}Ti_{0.99}Mg_{0.01}O_{3-\delta}$. Solid State Ion 360:115547. https://doi.org/10.1016/J.SSI.2020.115547

50. Mrharrab L, Nfissi A, Ababou Y, Belhajji M, Sayouri S, Faik A (2021) "Effect of starting materials on the structure of pure and Gd-doped $BaTiO_3$ elaborated by the sol gel process," Moroccan J Chem 9(4):628–638. https://doi.org/10.48317/IMIST.PRSM/morjchem-v9i4.27263

51. Elbasset A, Abdi F, Lamcharfi T-D et al. (2016) Characterization micro/nanostructures of barium strontium titanate. Orient J Chem 32(3):1521–1524

52. Wang X, Chan HLW, Choy CL (2003) "$(Bi_{1/2}Na_{1/2})TiO_3$-$Ba(Cu_{1/2}W$ $1/2)O_3$ lead-free piezoelectric ceramics,". J Am Ceram Soc 86(10):1809–1811. https://doi.org/10.1111/j.1151-2916.2003.tb03562.x

53. Hiruma Y, Aoyagi R, Nagata H, Takenaka T (2005) "Ferroelectric and piezoelectric properties of $(Bi_{1/2}K$ $1/2)TiO_3$ ceramics,". Jpn J Appl Phys, Part 1 Regul Pap Short Notes Rev Pap 44(7A):5040–5044. https://doi.org/10.1143/JJAP.44.5040

54. Chourti K et al. (2020) "Relationships between crystalline structure and dielectric properties in $Sr_2Sm_{(1-x)}$ $Nd_xTi_2Nb_3O_{15}$ ceramics,". Rev Imist Ma 8:304–317